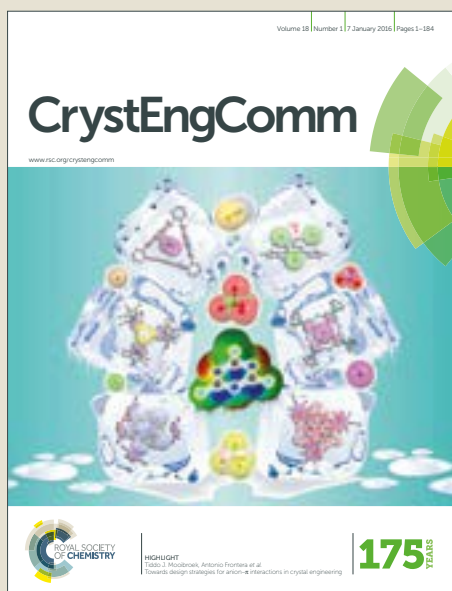


# CrystEngComm

Accepted Manuscript



This article can be cited before page numbers have been issued, to do this please use: M. Zhang, Z. Zheng, Q. Fu, Z. Chen, J. He, S. Zhang, L. Yan, Y. Hu and W. Luo, *CrystEngComm*, 2017, DOI: 10.1039/C7CE01709J.



This is an Accepted Manuscript, which has been through the Royal Society of Chemistry peer review process and has been accepted for publication.

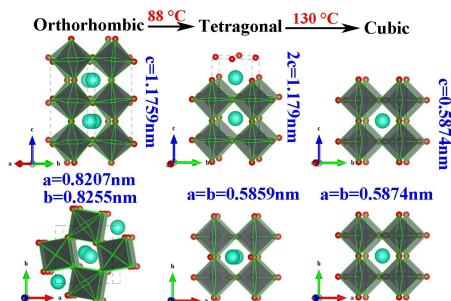
Accepted Manuscripts are published online shortly after acceptance, before technical editing, formatting and proof reading. Using this free service, authors can make their results available to the community, in citable form, before we publish the edited article. We will replace this Accepted Manuscript with the edited and formatted Advance Article as soon as it is available.

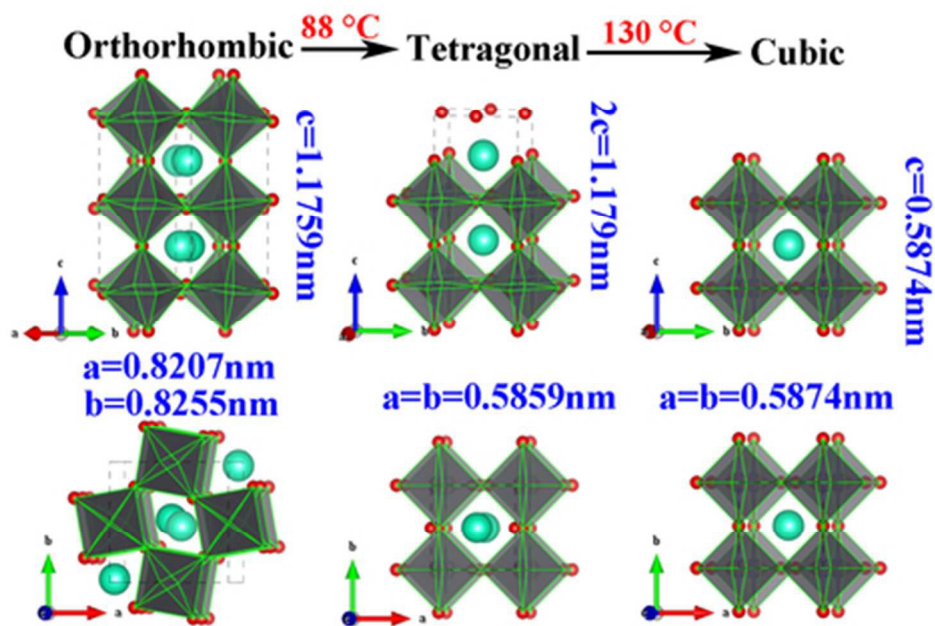
You can find more information about Accepted Manuscripts in the [author guidelines](#).

Please note that technical editing may introduce minor changes to the text and/or graphics, which may alter content. The journal's standard [Terms & Conditions](#) and the ethical guidelines, outlined in our [author and reviewer resource centre](#), still apply. In no event shall the Royal Society of Chemistry be held responsible for any errors or omissions in this Accepted Manuscript or any consequences arising from the use of any information it contains.

## Table of Contents (TOC) Entry

The crystal structure transform from orthorhombic to tetragonal at 88 °C and then to cubic at 130 °C.





The crystal structure transform from orthorhombic to tetragonal at 88 °C and then to cubic at 130 °C.

39x26mm (300 x 300 DPI)

Please do not adjust margins



## Journal Name

## ARTICLE

## Growth and characterization of the all-inorganic lead halide perovskite semiconductor CsPbBr<sub>3</sub> single crystals

Mingzhi Zhang,<sup>a</sup> Zhiping Zheng,<sup>a</sup> Qiyun Fu,<sup>a,b</sup> Zheng Chen,<sup>a</sup> Jianle He,<sup>a</sup> Sen Zhang,<sup>a</sup> Liang Yan,<sup>a</sup> Yunxiang Hu,<sup>a</sup> and Wei Luo<sup>a</sup>

Received 00th January 20xx,  
Accepted 00th January 20xx

DOI: 10.1039/x0xx00000x

www.rsc.org/

As a typical representative of all-inorganic lead halide perovskites, cesium lead bromine (CsPbBr<sub>3</sub>) has attracted significant attention in the context of photovoltaics and other optoelectronic applications in recent years. In this paper, CsPbBr<sub>3</sub> single crystal growth was conducted by a creative electro dynamic gradient (EDG) method. The crystal structure was systematic investigated by scientific instruments and equipment. X-ray diffraction techniques, including X-ray diffraction (XRD), temperature-dependent X-ray powder diffraction and X-ray rocking curve were used to identify phase and to investigate phase transition rules. Electron diffraction techniques, including high-resolution transmission electron microscopy (HRTEM), selected area electron diffraction (SAED) and electron backscatter diffraction (EBSD) were used to investigate crystal micro-structure. The final results indicated that the grown CsPbBr<sub>3</sub> crystal was a perfect single crystal preferentially orienting in the (110) direction and met the basic demand of applications.

### 1. Introduction

Lead halide perovskite materials have attracted significant attention in the context of photovoltaics and other optoelectronic applications in recent years. Demonstrated optoelectronic applications of lead halide perovskites include high-efficiency solar cells,<sup>1,2</sup> lasers,<sup>3,4</sup> light-emitting diodes (LED),<sup>5,6</sup> and high-gain photodetectors.<sup>7-10</sup> However organic-inorganic hybrid lead halide perovskite materials (the general formula APbX<sub>3</sub>) are often criticized for their inherent instability, such as high sensitivity to oxygen and moisture.<sup>11,12</sup>

These instability originated from the A-site organic cations or cationic clusters (MA<sup>+</sup>, FA<sup>+</sup> et. al).<sup>1-3,11,13</sup> Recently, more and more research efforts have been directed to all-inorganic lead halide perovskite,<sup>14-19</sup> which has better mechanical and moisture stability than organic-inorganic hybrid lead halide ones. Benefiting from their promising properties such as excellent optical performance, high charge carrier mobility and a general tolerance to defects, all-inorganic lead halide perovskites MPbX<sub>3</sub> (M=K, Rb, and Cs, X = I, Br, and Cl) have drawn much attention to them.<sup>20-22</sup> Furthermore, these all-

inorganic lead halide perovskites show nearly the same power conversion efficiency as the leading solar cell material, hybrid organic-inorganic CH<sub>3</sub>NH<sub>3</sub>PbI<sub>3</sub>.<sup>23</sup>

In this study, we turn readers' attention to one kind of all-inorganic lead halide perovskites, cesium lead bromine (CsPbBr<sub>3</sub>). CsPbBr<sub>3</sub> is an attractive detection medium for nuclear radiation in view of its relatively high density (4.84 g/cm<sup>3</sup>) and high average atomic number (Cs: 55, Pb: 82 and Br: 35). Additionally, its large band gap (2.25 eV) offers the possibility of low noise performance at room temperature. What is more, CsPbBr<sub>3</sub> has a same order of carrier mobility lifetime products for both electrons and holes (1.7×10<sup>-3</sup> cm<sup>2</sup>/V and 1.3×10<sup>-3</sup> cm<sup>2</sup>/V for electrons and holes, respectively),<sup>7</sup> implying that no special engineering methodologies are required for patching mismatches between holes and electrons. Thus, this ternary compound shows potential characteristic in the optoelectronic performance, especially in the high energy radiation detection.<sup>7,10</sup> However, the overwhelming majority of perovskite devices are based upon polycrystalline thin films, which suffer immensely from a high density of traps and grain boundaries. Compared with the polycrystalline CsPbBr<sub>3</sub> thin films, CsPbBr<sub>3</sub> single crystals display exceptionally low trap densities (6 orders of magnitude less compared to their polycrystalline films).<sup>24</sup> However, the available research on the structure and physical properties of the CsPbBr<sub>3</sub> single crystals is not very sufficient and many great blanks need to be filled. Therefore, the potential application of these polycrystalline devices is markedly limited. Although the synthesis, crystallography, and photoconductivity of all-inorganic lead halide perovskites have been first reported more than 50 years ago, few researchers have focused on the direct band-gap MPbX<sub>3</sub> single crystals until 2015.<sup>25</sup> Therefore,

<sup>a</sup> School of Optical and Electronic Information, Huazhong University of Science and Technology, Wuhan 430074, PR China, Corresponding author : Zhiping Zheng, Email: zzp@mail.hust.edu.cn, Fax: +86-27-87545167, Tel: +86-27-87545167,

<sup>b</sup> State Key Laboratory of Material Processing and Die & Mold Technology, Huazhong University of Science and Technology, Wuhan 430074, PR China.

Electronic Supplementary Information (ESI) available: Experimental details and Supporting Figures.

Please do not adjust margins

Please do not adjust margins

ARTICLE

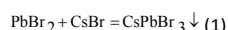
Journal Name

the growing interest in perovskite single crystals motivated us to develop facile methods for the single crystal growth of CsPbBr<sub>3</sub>.<sup>7,10,14,26</sup>

## 2. Experimental

### 2.1 Synthesis of CsPbBr<sub>3</sub> polycrystalline powders

Synthesis of the CsPbBr<sub>3</sub> polycrystalline powders was carried out by chemical co-precipitation method.<sup>27</sup> Commercial available lead (II) bromide (PbBr<sub>2</sub>, 99.999%) and cesium bromide (CsBr, 99.999%) were supplied by Alfa Aesar (Sain Louis, UK). Aqueous hydrobromic acid (HBr, 48 wt% in H<sub>2</sub>O, 99.99% metals basis) was purchased from Aladdin (Shanghai, China). PbBr<sub>2</sub> (20 mmol, 7.34g) and CsBr (20 mmol, 4.26g) were respectively dissolved in the hydrobromic acid [48% HBr(aq)] in separate beakers to form PbBr<sub>2</sub> and CsBr solutions in advance. Then the solutions were simultaneously dropwise added into 5 ml of 48% aqueous HBr with stirring during the synthesis reaction. The precipitation reaction was as following:



Bright orange precipitation of CsPbBr<sub>3</sub> immediately formed in the aqueous HBr solution. The precipitation was filtered, copiously rinsed three times by absolute ethyl alcohol and then dried under vacuum to obtain orange CsPbBr<sub>3</sub> polycrystalline powders.

### 2.2 A tube furnace and EDG crystal growth

The thermogravimetric analysis of the CsPbBr<sub>3</sub> powders was described in supporting information (Supporting Information 1.1 and Figure S1-S2). The melting point and solidifying point was 567 °C and 550 °C according to Figure S1. The melting point has the same result as the reported in Ref 7, but the solidifying point had a slight deviation. This deviation maybe come from the different degree of supercooling under diverse testing conditions (rate of temperature rise, protective atmosphere etc.). The reported crystal structure transitions from the orthorhombic (Pnma) to the tetragonal (P4/mbm) symmetries and from tetragonal (P4/mbm) to cubic (Pm-3m) were not observed in our analysis, possibly due to insufficient sensitivity of the measurement.<sup>7,14,28</sup> The single crystal growth was conducted in a self-designed vertical two-zone tube furnace by a simplified electronic dynamic gradient (EDG) method.<sup>29</sup> The detailed procedure of CsPbBr<sub>3</sub> crystal growth was described in supporting information (Supporting Information 1.2 and Figure S3).

### 2.3 Structural characterization

The crystal structure was systematically investigated by scientific instruments and equipments. A BRUKER AXS D8 ADVANCE X-ray diffractometer equipped with heating system was used to characterize the phase identification of the crystal. The rocking curve was tested in  $\omega$  scan mode using CuK1 source with a wavelength of 1.5406 Å, under a generator voltage of 40 kV, and a generator current of 40 mA. Selected area electron diffraction (SAED) and high-resolution

transmission electron microscopy (HRTEM) were performed using a Tecnai F30 G2 electron microscope with an incident electron energy of 300 keV. The micro-structural crystallographic characterization of the crystal was investigated by EBSD patterns using accelerating voltage of 20 kV by a FEI Nova Sirion 200.

### 2.4 Optical characterization

The quality of the crystal was mainly characterized by the optical performance. The optical transmittance was studied by Bruker Vertex70 FT-IR (wavenumber range 1000-4000 cm<sup>-1</sup>) and Perkin-Elmer Lambda 35 Ultraviolet spectrophotometer (wavelength range 190-2600 nm) at room temperature.

## 3. Result and discussion

### 3.1 Phase identification of CsPbBr<sub>3</sub> powder

The powder XRD patterns of the synthesized polycrystalline powders, together with the standard patterns of cubic phase (ICSD 29073, Pm-3m(221), a=b=c=0.5874 nm)<sup>30</sup> and orthorhombic phase (ICSD 97851, Pbnm(62), a=0.8207 nm, b=0.8255 nm, c=1.1759 nm)<sup>31</sup> of CsPbBr<sub>3</sub> were shown in Figure 1. The standard patterns of tetragonal phase (ICSD 109295, P4/mbm(99), a=b=0.5859 nm, c=0.5895 nm)<sup>32</sup> were shown in Figure S4. It was illustrated that the first three strong peaks of the synthesized polycrystalline powders, (110) at 15.198°, (112) at 21.443° and (220) at 30.663°, matched up with the standard orthorhombic perovskite structure well. Thus the synthesized powders can be identified as CsPbBr<sub>3</sub> powders. Meanwhile the clear splitting of (110) and (220) diffraction peaks further indicated that the synthesized CsPbBr<sub>3</sub> polycrystalline powders may be of room-temperature orthorhombic phase (Pbnm),<sup>3</sup> but further study was needed to prove it.

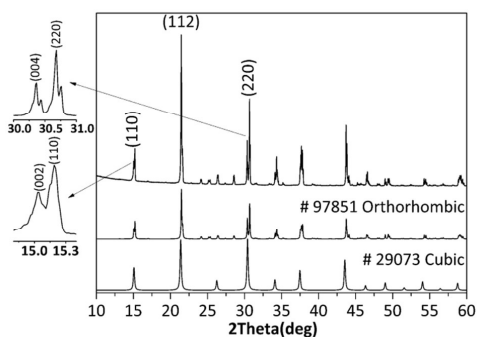


Figure 1 Powder X-ray diffraction patterns of the synthesized powders and the split diffraction peaks

In order to further study the final phase of CsPbBr<sub>3</sub> crystal, a small portion of the grown CsPbBr<sub>3</sub> ingot was ground into fine powders. Then temperature-dependent powder X-ray diffraction was used to study the phase transitions of CsPbBr<sub>3</sub>,

Please do not adjust margins

Please do not adjust margins

Journal Name

ARTICLE

and the results were shown in Figure 2, with the standard patterns of cubic (ICSD 29073), tetragonal (ICSD 109295) and orthorhombic (ICSD 97851) perovskite structure shown in the top, middle and bottom of the figure, respectively. Obviously, the crystal structure of CsPbBr<sub>3</sub> changed with the temperature increasing from room temperature (300 K) to high temperature (500 K). Splitting of the strong diffraction peaks disappeared gradually with the temperature increasing. And the weak diffraction peaks at 24.165°, 25.347°, 28.587° (the featured peaks of low temperature phase) also disappeared gradually with the temperature increasing. These phenomena can be observed more clearly in the zoom-in image of the XRD pattern, which shown in supporting information (Supporting Information 1.3 and Figure S5). These phenomena indicated that the phase transitions of CsPbBr<sub>3</sub> were occurred with temperature rise and the phase transition temperatures were around 360 K (87 °C) and 400 K (127 °C). According to Ref 7, CsPbBr<sub>3</sub> had two successive phase transitions at 88 °C and 130 °C, corresponding to the crystal structure transforming from room temperature orthorhombic (Pbnm, equal to Pnma) to tetragonal (P4/mbm) and then to cubic (Pm-3m), respectively. The temperature-dependent XRD patterns of this work were similar to that reported in Ref.7. The orthorhombic phase (Pbnm) had a typical characteristic of splitting diffraction peaks at 15.198° and 30.663° relative to the cubic phase (Pm-3m).<sup>3</sup>

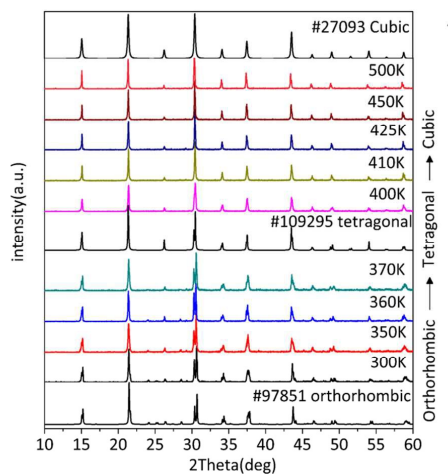


Figure 2 Temperature-dependence X-ray powder diffraction patterns of CsPbBr<sub>3</sub> powders

### 3.2 General appearance of CsPbBr<sub>3</sub> single crystal

An as-grown CsPbBr<sub>3</sub> crystal with 60 mm overall length was obtained from EDG method. The conical part of the crystal ingot was about 30 mm in length as shaped by the ampule, and it was irregular with a gradually varied diameter. The isometric part, with a diameter of 8 mm and an approximate length of 30 mm, was sliced into wafers to investigate the

phase and the quality of the crystal. The fabrication of wafers was described in supporting information (Supporting Information 1.4). Figure S6 presented a photograph of the isometric part of the crystal ingot. Figure 3 showed a photograph of a typical wafer with 8 mm in diameter and 1.5 mm in thickness. Obviously, the wafer had orange yellow color, a good transparency and a bright, shiny and mirror-like surface.

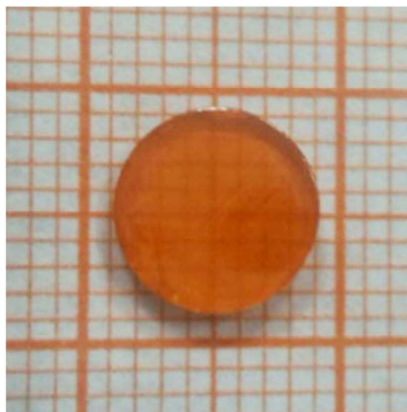
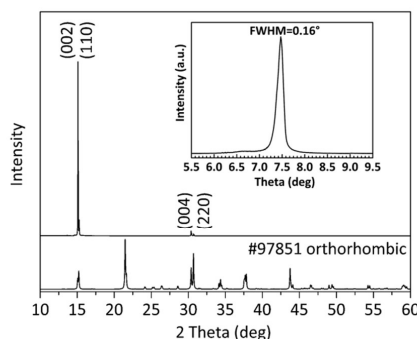


Figure 3 Photograph of a CsPbBr<sub>3</sub> wafer

### 3.3 X-ray diffraction and rocking curve analysis

Figure 4 presented the XRD pattern of a CsPbBr<sub>3</sub> wafer, with the standard pattern of the orthorhombic structure (ICSD 97851) provided at the bottom. It can be seen that the intensity of the (110) peak was quite strong, indicating that the crystal was a perfect single crystal preferentially orienting in the (110) direction. The secondary diffraction peak of (220) plane suggested crystalline perfection. The clear splitting of (110) and (220) peaks indicated that the grown CsPbBr<sub>3</sub> crystal was of the room-temperature orthorhombic phase.<sup>3</sup>



Please do not adjust margins

Please do not adjust margins

## ARTICLE

Journal Name

Figure 4 XRD pattern and rocking curve of the (110) plane of the crystal, inset: rocking curve

To further study the crystalline quality of the crystal, the X-ray rocking curve of the (110) plane was measured, as inserted in Figure 4. Evidently, the curve was a primarily symmetric single peak without any split peaks, which meant there was no twinning in the crystal. The full width at half-maximum (FWHM) of the (110) peak of the rocking curve was  $0.16^\circ$ . The relatively small FWHM of the crystal indicated a low dislocation density and small residual stress in the crystal.

### 3.4 Electron diffraction analysis

Considering the detection limit of XRD measurements (concentration > 5%),<sup>33</sup> the purity of orthorhombic phase was still in doubt. Then high resolution TEM (HRTEM) technology was used to analyze the micro-structure of the crystal. A typical HRTEM image of the CsPbBr<sub>3</sub> single crystal observed at room temperature was shown in Figure 5. A fast Fourier transform (FFT) image of the HRTEM image was inset in Figure 5. The well-regulated arrayed spots indicated the grown crystal had a perfect quality without twinning, dislocation and stacking fault. The interplanar distances of the orthogonal directions in HRTEM image were 0.582 nm and 0.586 nm, respectively. Meanwhile, the interplanar distances of the orthogonal directions in FFT image were calculated as 0.58 nm and 0.595 nm, respectively. As the diffraction spots in FFT image were of low resolution, it is hard to distinguish the cubic phase from the orthorhombic one. Therefore more clear and detailed diffraction spots were needed.

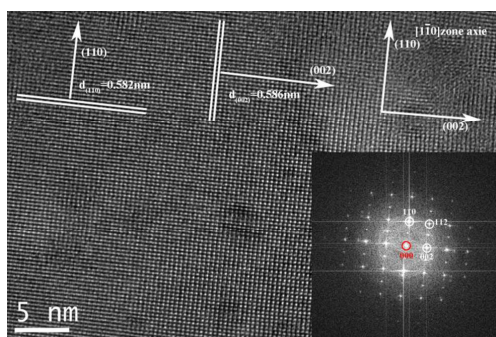


Figure 5 Typical HRTEM and FFT images of the CPB crystal, inset: FFT image

A selected area electron diffraction (SAED) image of the CsPbBr<sub>3</sub> single crystal was shown in Figure 6. Two reciprocal lattice primitive vectors in the SAED image, with a length of 1.72 1/nm (0.581 nm in direct lattice) and 1.70 1/nm (0.588 nm in direct lattice), were rectangular. Other two reciprocal lattice vectors, with a length of 1.92 1/nm (0.52 nm in direct lattice) and 3.85 1/nm (0.26 nm in direct lattice) were measured from

weak spots (111) and (222) (marked by blue circles), which were unique for the orthorhombic (ICSD 97851) phase and were missing in the cubic (ICSD 29073) and tetragonal (ICSD 109295) phases. The weak and unique spots help to distinguish the orthorhombic from the cubic phase.<sup>34,35</sup>

Therefore the HRTEM and SAED image analyses revealed that the CsPbBr<sub>3</sub> single crystal had a structure matching with an orthorhombic crystal phase (ICSD 97851, Pbnm (62),  $a = 8.207 \text{ \AA}$ ,  $b = 8.255 \text{ \AA}$ ,  $c = 11.759 \text{ \AA}$ ), which was also reported by Zhang *et al.*<sup>36</sup> for CsPbBr<sub>3</sub> nanowires<sup>31</sup>, and by Abhishek Swarnkar *et al.*<sup>37</sup> and Cottingham *et al.*<sup>38</sup> for CsPbBr<sub>3</sub> nanocuboids. The crystal was along the  $[1\bar{1}0]$  zone axis and the spots (002), (112), (111) and (110) were in the same plane (see Figure 6(a)). The vectorial angles among the diffraction spots (002), (112), (111) and (110) were  $45.3^\circ$ ,  $18.4^\circ$  and  $26.3^\circ$ , respectively, as marked in Figure S7. Figure 6(b) showed the standard reciprocal lattice patterns of the orthorhombic (ICSD 97851) and the cubic (ICSD 29073) CsPbBr<sub>3</sub> phases, respectively.

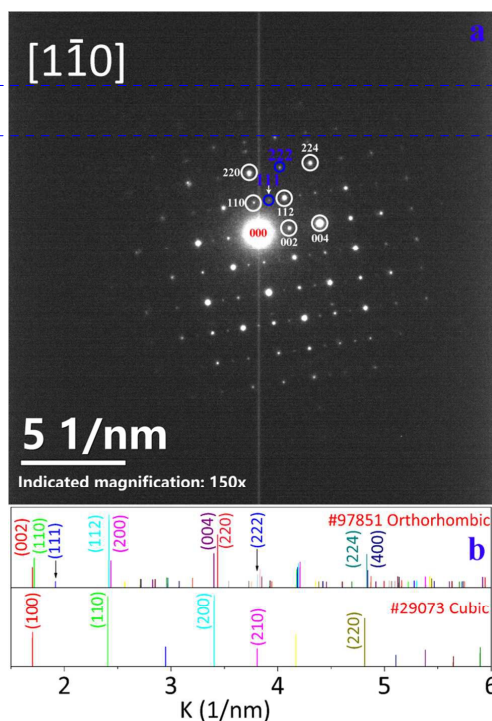


Figure 6 SAED pattern of the CsPbBr<sub>3</sub> crystal along the  $[1\bar{1}0]$  zone axis: (a) SAED pattern; (b) standard patterns for the orthorhombic (ICSD 97851) and the cubic (ICSD 29073) phases

In order to identify the crystallographic orientations and domains of the crystal, the micro-structure crystallographic

Formatted: Font: 9 pt

Formatted: Font: 9 pt

Formatted: Font: 9 pt

CrystEngComm Accepted Manuscript

Please do not adjust margins

Please do not adjust margins

Journal Name

ARTICLE

was further analyzed by electron backscatter diffraction (EBSD)<sup>39,40</sup>. EBSD is a SEM based micro-structural crystallographic characterization technique that is well established to determine the crystallographic orientations, texture, defects, grain morphology and deformation of micro-structures. In this technique, the focused electron beam strikes the surface of the crystal at a high angle (here, 70°). Backscatter diffraction electrons scattered from the surface form a diffraction pattern, called a Kikuchi pattern because of its prominent Kikuchi bands. Before the EBSD measurement, wafer surfaces were etched by argon ions for 30 min to smooth and clean the wafer. Figure 7 showed the surface topography and micro-structural crystallographic orientation of a CsPbBr<sub>3</sub> crystal wafer. As labelled in Figure 7(a), an area of 900 × 900 μm<sup>2</sup> on the CsPbBr<sub>3</sub> wafer surface was selected for EBSD pattern measurement. The corresponding EBSD patterns (Kikuchi patterns) were shown in Figure 7(b). Remarkably, these patterns were similar, indicating the same crystallographic orientation and no grain boundaries within the crystal. Figure 7(c) showed the crystallographic orientation map with the standard colour orientation reference system inserted. The crystallographic orientation map was formed by the numbers of Kikuchi patterns through statistical analysis. A specific color represented a specific orientation. Clearly, the map showed nearly the same color, indicating the crystal had a single orientation. And this single orientation was confirmed by the inverse pole figure (IPF) map as shown in Figure 7(d). The concentrated point in the inverse pole figure (IPF) indicated the crystal was a perfect single oriented crystal. More information about characterization of EBSD pattern on various regions from the edge to center of the wafer was described in supporting information (Figure S8-9).

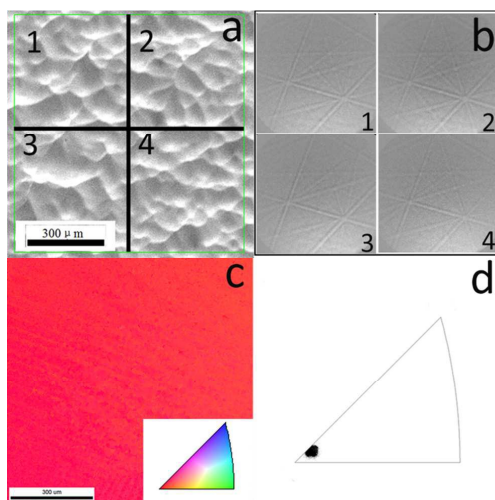


Figure 7 Microstructure and crystallographic orientation map of a CsPbBr<sub>3</sub> crystal (a) SEM image, (b) Kikuchi patterns, (c)

crystallographic orientation map, and (d) Inverse pole figure (IPF) map.

### 3.5 Optical characterization

The IR and UV-Vis-NIR transmittance spectra of the wafer were shown in Figure 8(a) and (b), respectively. A high IR transmittance over 55% at the whole spectrum region was observed. Since the IR average transmittance was mainly affected by point defects, vacancies and impurities in the crystal, the high IR average transmittance meant low defect density in the crystal.<sup>41,42</sup> Two absorption peaks were found clearly at about 1600 cm<sup>-1</sup> and 3500 cm<sup>-1</sup> in the transmittance spectrum, and they were regarded as the infrared absorption peaks of water vibrational modes in the atmosphere.<sup>43,44</sup> The wafer also possessed a high transmittance in the UV-Vis-NIR region, as shown in Figure 8(b). The good optical performance indicated that the crystal had a high purity and a good crystal quality. Furthermore, the absorption edge of the wafer was found to be at 550 nm in the UV-Vis-NIR transmittance spectrum.<sup>7, 10,45</sup> The band gap of the crystal was calculated to be approximately 2.252 eV according to the equation:

$$E_g = \frac{h \cdot c}{\lambda_e}$$

where the  $\lambda_e$  was the absorption edge wavelength. The result was in line with the data reported in Ref 7.

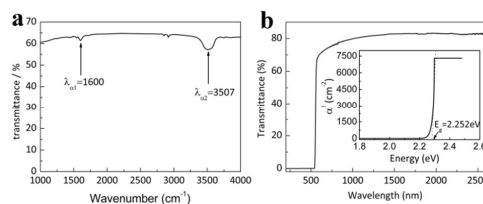


Figure 8 (a) IR transmittance spectrum and (b) UV-Vis-NIR transmittance spectrum of a CsPbBr<sub>3</sub> wafer

## 4. Conclusions

In this paper, CsPbBr<sub>3</sub> polycrystalline powders were synthesized by a chemical co-precipitation method. CsPbBr<sub>3</sub> single crystal of 8 mm diameter and 60 mm overall length was successfully grown by a facile melt-method (EDG method). The phase transitions and micro-structure were systematic investigated by scientific instruments and equipment. The temperature-dependent powder XRD patterns indicated CsPbBr<sub>3</sub> had two successive phase transitions at around 88 °C and 130 °C, corresponding to the crystal structure transforming from room temperature orthorhombic (62, Pbnm, equal to Pnma) to tetragonal (99, P4/mbm) and then to cubic (221, Pm-3m), respectively. The XRD patterns showed that the crystal was a single crystal preferentially orienting in the (110) direction. The X-ray rocking curve of (110) plane showed a sharp peak with a FWHM of 0.16°, indicating a low dislocation

Please do not adjust margins

Please do not adjust margins

## ARTICLE

## Journal Name

density and residual stress in the crystal. HRTEM image showed the high quality of the crystal without twinning, dislocation and stacking fault. FFT and SAED image indicated the crystal had a pure room-temperature orthorhombic phase. The results of EBSD confirmed that CsPbBr<sub>3</sub> crystal was a perfect single crystal along single orientation with no grain boundaries. The crystal showed good transparency with a high IR and UV-Vis-NIR transmittance. The above results proved that the EDG method was a feasible and effective method to grow perfect CsPbBr<sub>3</sub> single crystals.

## Acknowledgements

This work was financially supported by the National Natural Science Foundation of China under Grant Nos. 11575065 and 11275078. The authors acknowledge the assistance of the Analytical and Testing Center (ATC) and State Key Laboratory of Material Processing and Die & Mold Technology of Huazhong University of Science and Technology (HUST). The authors also wish to express their hearty thanks to School of Physics and Technology of Wuhan University for X-ray rocking curve testing.

## Notes and references

- C. Yi, J. Luo, S. Meloni, A. Boziki, N. Ashari-Astani, C. Grätzel, S. M. Zakeeruddin, U. Röthlisberger and M. Grätzel, *Energy Environ. Sci.*, 2016, **9**(2), 656–662.
- M. Kulbak, S. Gupta, N. Kedem, I. Levine, T. Bendikov, G. Hodes and D. Cahen, *J. Phys. Chem. Lett.*, 2016, **7**(1), 167–172.
- S. W. Eaton, M. Lai, N. A. Gibson, A. B. Wong, L. Dou, J. Ma, L. W. Wang, S. R. Leone and P. Yang, *PNAS*, 2016, **113**(8), 1993–1998.
- Y. Xu, Q. Chen, C. Zhang, R. Wang, H. Wu, X. Zhang, G. Xing, W. W. Yu, X. Wang, Y. Zhang and M. Xiao, *J. Am. Chem. Soc.*, 2016, **138**(11), 3761–3768.
- H. Cho, S. H. Jeong, M. H. Park, Y. H. Kim, C. Wolf, C. L. Lee, A. Sadhanala, N. S. Myoung, S. Yoo, S. H. Im, R. H. Friend and T. W. Lee, *Science*, 2015, **350**(6265), 1222–1225.
- X. Zhang, H. Lin, H. Huang, C. Reckmeier, Y. Zhang, W. C. Choy and A. L. Rogach, *Nano Lett.*, 2016, **16**(2), 1415–1420.
- C. C. Stoumpos, C. D. Malliakas, J. A. Peters, Z. Liu, M. Sebastian, J. Im, T. C. Chasapis, A. C. Wibowo, D. Y. Chung, A. J. Freeman, B. W. Wessels and M. G. Kanatzidis, *Cryst. Growth Des.*, 2013, **13**(7), 2722–2727.
- L. Lv, Y. Xu, H. Fang, W. Luo, F. Xu, L. Liu, B. Wang, X. Zhang, D. Yang, W. Hu and A. Dong, *Nanoscale*, 2016, **8**(28), 13589–13596.
- L. Gao, K. Zeng, J. Guo, C. Ge, J. Du, Y. Zhao, C. Chen, H. Deng, Y. He, H. Song, G. Niu and J. Tang, *Nano Lett.*, 2016, **16**(12), 7446–7454.
- D. N. Dirin, I. Cherniukh, S. Yakunin, Y. Shynkarenko and M. V. Kovalenko, *Chem. Mater.*, 2016, **28**(23), 8470–8474.
- X. Zhang, B. Xu, W. Wang, S. Liu, Y. Zheng, S. Chen, K. Wang and X. W. Sun, *ACS Appl. Mater. Interfaces*, 2017, **9**(5), 4926–4931.
- K. A. Bush, C. D. Bailie, Y. C. Andrea, R. Bowring, W. Wang, W. Ma, T. Leijtens, F. Moghadam and M. D. McGehee, *Adv. Mater.*, 2016, **28**(20), 3937–3943.
- X. He, Y. Qiu and S. Yang, *Advanced materials*, 2017, **29**(32), 1700775.
- Y. Rakita, N. Kedem, S. Gupta, A. Sadhanala, V. Kalchenko, M. L. Böhm, M. Kulbak, R. H. Friend, D. Cahen and G. Hodes, *Cryst. Growth Des.*, 2016, **16**(10), 5717–5725.
- G. P. Li, H. Wang, Z. F. Zhu, Y. J. Chang, T. Zhang, Z. H. Song and Y. Jiang, *Chem. Commun.*, 2016, **52**(75), 11296–11299.
- P. Ramasamy, D. H. Lim, B. Kim, S. H. Lee, M. S. Lee and J. S. Lee, *Chem. Commun.*, 2016, **52**(10), 2067–2070.
- J. De Roo, M. Ibanez, P. Geiregat, G. Nedelcu, W. Walravens, J. Maes, J. C. Martins, I. Van Driessche, M. V. Kovalenko and Z. Hens, *ACS Nano*, 2016, **10**(2), 2071–2081.
- Y. Wang, X. Li, X. Zhao, L. Xiao, H. Zeng and H. Sun, *Nano Lett.*, 2016, **16**(1), 448–453.
- S. Seth, N. Mondal, S. Patra and A. Samanta, *J. Phys. Chem. Lett.*, 2016, **7**(2), 266–271.
- Q. A. Akkerman, S. G. Motti, A. R. Srimath Kandada, E. Mosconi, V. D'Innocenzo, G. Bertoni, S. Marras, B. A. Kamino, L. De Miranda, F. Angelis, A. Petrozza, M. Prato and L. Manna, *J. Am. Chem. Soc.*, 2016, **138**(3), 1010–1016.
- I. Chung, B. Lee, J. He, R. P. Chang and M. G. Kanatzidis, *Nature*, 2012, **485**(7399), 486–489.
- L.-y. Huang and W. R. L. Lambrecht, *Phys. Rev. B.*, 2016, **93**(19), 195211.
- M. Kulbak, D. Cahen and G. Hodes, *J. Phys. Chem. Lett.*, 2015, **6**(13), 2452–2456.
- M. I. Saidaminov, A. L. Abdelhady, G. Maculan and, O. M. Bakr, *Chem. Commun.*, 2015, **51**(100), 17658–17661.
- C. K. Møller, *Nature*, 1958, **182**(4637), 1436–1436.
- X. Ding, S. j. Du, Z. Y. Zuo, Y. G. Zhao, H. Z. Cui and X. Y. Zhan, *J. Phys. Chem. C*, 2017, **121**(9), 4917–4923.
- D. X. Zhou, L. Quan, X. Chen, S. Yu, Z. Z. Zheng and S. P. Gong, *J. Cryst. Growth*, 2009, **311**(8), 2524–2529.
- M. Rodová, J. Brožek, K. Knížek and K. Nitsch, *J. Therm. Anal. Calorim.*, 2003, **71**(2), 667–673.
- D. X. Zhou, L. Quan, X. Y. Chen, S. J. Yu, C. Wang, Z. Z. Zheng, and S. P. Gong, *Cryst. Growth Des.*, 2009, **9**(10), 4296–4300.
- H. Huang, M. Liu, J. Li, L. Luo, J. Zhao, Z. Luo, X. Wang, Z. Ye, H. He and J. Zeng, *Nanoscale*, 2017, **9**(1), 104–108.
- M. Imran, F. Di Stasio, Z. Dang, C. Canale, A. H. Khan, J. Shamsi, R. Brescia, M. Prato and L. Manna, *Chem. Mater.*, 2016, **28**(18), 6450–6454.
- J. Zhao, M. Liu, L. Fang, S. Jiang, J. Zhou, H. Ding, H. Huang, W. Wen, Z. Luo, Q. Zhang, X. Wang and C. Gao, *J. Phys. Chem. Lett.*, 2017, **8**(13), 3115–3121.
- L. Luo, W. Jie, Y. Xu, Y. He, L. Xu and L. Fu, *CrystEngComm*, 2014, **16**(23), 5073–5079.
- Z. Dang, R. Brescia, Q. Akkerman, J. Shamsi, M. Prato and L. Manna, *European Microscopy Congress 2016: Proceedings*, 2016, 530–531.
- J. Shamsi, Z. Dang, P. Bianchini, C. Canale, F. D. Stasio, R. Brescia, M. Prato and L. Manna, *J. Am. Chem. Soc.*, 2016, **138**(23), 7240–7243.
- D. Zhang, S. W. Eaton, Y. Yu, L. Dou and P. Yang, *J. Am. Chem. Soc.*, 2015, **137**(29), 9230–9233.
- A. Swarnkar, R. Chulliyil, V. K. Ravi, M. Irfanullah, A. Chowdhury and A. Nag, *Angew. Chem., Int. Ed.*, 2015, **54**(51), 15424–15428.
- P. Cottingham and R. L. Brutchey, *Chem. Commun*, 2016, **52**(30), 5246–5249.
- P. Khoram, S. Brittman, W. I. Dzik, J. N. H. Reek and E. C. Garnett, *J. Phys. Chem. C.*, 2016, **120**(12), 6475–6481.
- S. K. Sundaram, C. H. Henager, D. J. Edwards, A. L. Scherer-Kohn, M. Bliss and B. R. Riley, *Journal of Crystal Growth*, 2011, **329**(1), 12–19.
- J. Min, X. Liang, J. Chen, D. Wang, H. Li and J. Zhang, *Vacuum*, 2012, **86**(7), 1003–1006.
- S. Yu, D. Zhou, S. Gong, Z. Zheng, Y. Hu, C. Wang and L. Quan, *Nuclear Instruments and Methods in Physics Research*

Please do not adjust margins

Please do not adjust margins

## Journal Name

## ARTICLE

*Section A: Accelerators, Spectrometers, Detectors and Associated Equipment*, 2009, **602(2)**, 484-488.

- 43 K. Ataka, T. Yotsuyanagi and M. Osawa, *J. Phys. Chem.*, 1996, **100(25)**, 10664-10672.
- 44 M. Osawa, M. Tsushima, H. Mogami, G. Samjeske and A. Yamakata, *J. Phys. Chem. C*, 2008, **112(11)**, 4248-4256.
- 45 M. I. Saidaminov, M. A. Haque, J. Almutlaq, S. Sarmah, X. H. Miao, R. Begum, A. A. Zhumekenov, I. Dursun, N. Cho, B. Murali, O. F. Mohammed, T. Wu and O. M. Bakr, *Adv. Opt. Mater.*, 2017, **5(2)**, 1600704.

Please do not adjust margins